ACS APPLIED MATERIALS & INTERFACES

www.acsami.org

Research Article

Bottlebrush Polymer-Conjugated Melittin Exhibits Enhanced Antitumor Activity and Better Safety Profile

Fei Jia,[§] Peiru Chen,[§] Dali Wang, Yehui Sun, Mengqi Ren, Yuyan Wang, Xueyan Cao, Lei Zhang, Yang Fang, Xuyu Tan, Hao Lu, Jiansong Cai, Xueguang Lu,* and Ke Zhang*

Cite This: *ACS Appl. Mater. Interfaces* 2021, 13, 42533−42542

Read Online

ACCESS | Metrics & More | Article Recommendations | Supporting Information

ABSTRACT: Despite potency against a variety of cancers in preclinical systems, melittin (MEL), a major peptide in bee venom, exhibits non-specific toxicity, severe hemolytic activity, and poor pharmacological properties. Therefore, its advancement in the clinical translation system has been limited to early-stage trials. Herein, we report a biohybrid involving a bottlebrush-architectured poly(ethylene glycol) (PEG) and MEL. Termed pacMEL, the conjugate consists of a high-density PEG arrangement, which provides MEL with steric inhibition against protein access, while the high molecular weight of pacMEL substantially enhances plasma pharmacokinetics with a ∼10-fold increase in the area under the curve (AUC_∞) compared to free MEL. pacMEL also significantly reduces hepatic damage and unwanted innate immune response and all but eliminated hemolytic activities of MEL. Importantly, pacMEL passively accumulates at subcutaneously inoculated tumor sites and exhibits stronger tumor-suppressive activity than molecular MEL. Collectively, pacMEL makes MEL a safer and more appealing drug candidate.

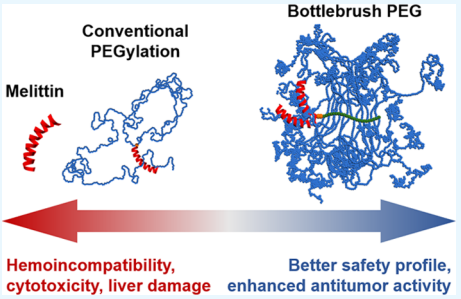

KEYWORDS: *melittin, bottlebrush polymer, drug delivery, PEGylation, narrow therapeutic index drugs*

INTRODUCTION

High binding constants and exquisite specificity with the target protein of peptides often give rise to great potencies and few off-target effects compared with conventional small-molecule drugs.[1−3] Still, only a small fraction of peptides with in vitro potency eventually achieves regulatory approval, largely due to the intrinsic low protease stability, rapid renal clearance, and side effects. For instance, melittin (MEL), a lytic peptide with promising antitumor activities, is severely limited by its difficult pharmacological properties and extensive hemolytic activity. Consisting of 26 amino acids, MEL is the main component of bee venom (∼50% dried weight). MEL can disrupt the phospholipid bilayer by generating transmembrane pores and cause the apoptosis/necrosis of cells. Importantly, MEL is regarded as one of the most potent anticancer agents as resistance against physical pore formation on the cell membrane is very difficult to develop by the cancer cell.[4−8] However, at therapeutic concentrations, which are barely above the sublytic concentrations, MEL causes significant side effects including hemolysis, coagulopathy, allergic reactions, and pain at the injection site, which would render MEL a narrow therapeutic index drug, with slight changes in dosage inducing therapeutic failures or severe adverse drug reactions.[9,10]

Observing these obstacles, we recognize that most of them are associated with unwanted interactions during initial systematic circulation, such as those with proteins in the coagulation pathway (coagulopathy), the red blood cell membrane (hemolysis), and immune cells (allergic reactions).[11−13] Suppressing these interactions may therefore reduce associated side effects, establish a new biodistribution profile that potentially redirects bioactivity of MEL to tissues of interest, and improve the therapeutic index. Covalent conjugation with the synthetic polymer poly(ethylene glycol) (PEG) is a clinically successful strategy to reduce unwanted interactions between the therapeutic agent and the biological environment, which has been adopted in more than 20 approved peptide/protein biopharmaceuticals since the approval of ADAGEN, a PEGylated adenosine deaminase.[14] PEG works by creating a large hydration shell shielding the conjugated species.[15,16] Conventional PEGylation with linear or slightly branched PEG has not been able to fully overcome the various toxicity challenges associated with MEL, in part due to insufficient shielding and the strong lytic properties of the peptide.[17] Recently, the rapid progress in polymer synthetic approaches allows polymers with more complex architectures to be obtained, such as the bottlebrush polymers, which can be easily synthesized by ring-opening metathesis polymerization.[18−20] Consisting of multiple PEG chains

Received: July 27, 2021
Accepted: August 18, 2021
Published: September 2, 2021

Scheme 1. Chemical Structures and Schematic Illustrations of PEGylated MELs

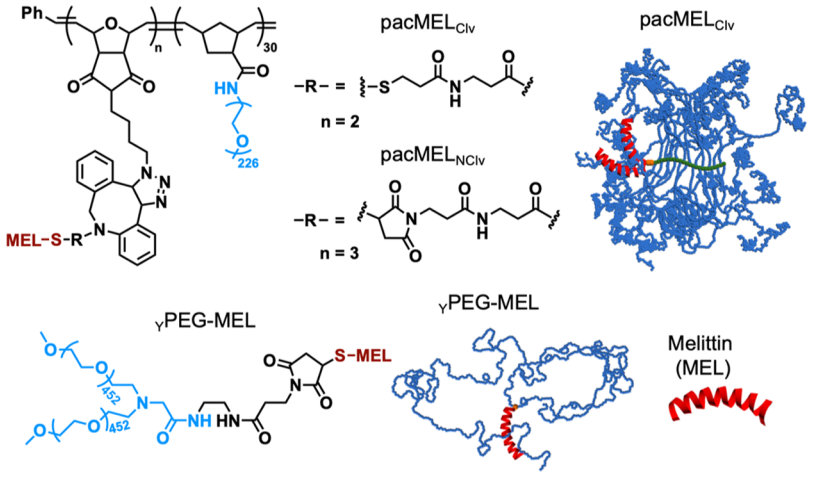

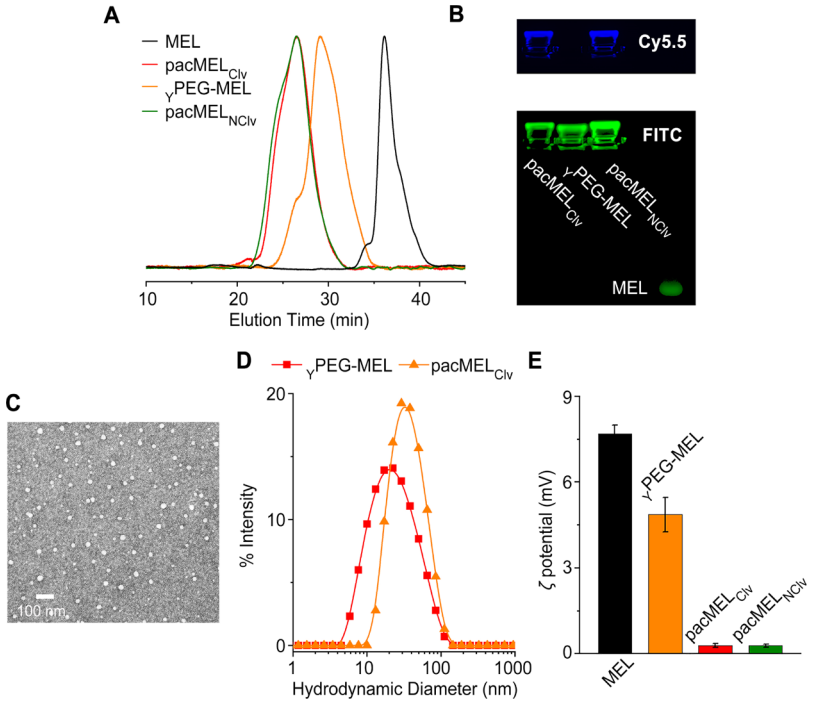

Figure 1. (A,B) Aqueous GPC chromatograms and agarose gel electrophoresis of purified PEGylated MELs and free MEL. Note that the GPC peaks for the conjugates display high molecular shoulders (more notable for $_Y$PEG-MEL), which suggest that the MEL component may cause slight aggregation. This peak asymmetry is absent for the parent brush polymer (Figure S2). (C) TEM image of pacMEL$_{Clv}$ negatively stained with 1% uranyl acetate. (D) Size distributions of PEGylated MELs (DLS intensity average; experiments were carried out at a scattering angle of 90° at room temperature in NanoPure water). (E) ζ-potential of free MEL and PEGylated MELs in NanoPure water.

(usually 15−30) densely arranged on a central polymer backbone, the bottlebrush PEG creates significantly greater spatial congestion than linear or slightly branched PEG, which makes it particularly suitable for steric shielding of highly promiscuous binders, membrane disruptive agents, and/or enzymatically vulnerable molecules (such as unmodified oligonucleotides).[21−26] Additionally, the recently reported degradable polynorbornene-based bottlebrush polymers further alleviate the concerns over using these large molecules as drug delivery vectors.[27,28]

Herein, we report a bottlebrush PEG-MEL conjugate as a non-immunogenic, non-hemolytic, and long-circulating antitumor prodrug to treat non-small-cell lung carcinoma (NSCLC) in a xenograft mouse model. Abbreviated as pacMEL (polymer-assisted compaction of MEL), the conjugate links approximately two molecules of MEL covalently to the backbone of the bottlebrush PEG via a bioreductively cleavable disulfide linker or a non-cleavable bond (Scheme 1). With reduced interactions with blood components, pacMEL exhibits markedly prolonged plasma pharmacokinetics (~21 × longer elimination half-life compared with free MEL) and elevated plasma availability [~10 × greater area under the curve (AUC_∞)], which promotes the passive targeting of tumor xenografts via the enhanced permeability and retention (EPR) effect. At a dosage where free MEL has no discernible effect on tumor growth, pacMEL is able to exert a significant tumor-suppressive activity. Importantly, pacMEL does not exhibit the typical toxicity profile of MEL, such as hemolytic

https://doi.org/10.1021/acsami.1c14285
ACS Appl. Mater. Interfaces 2021, 13, 42533−42542

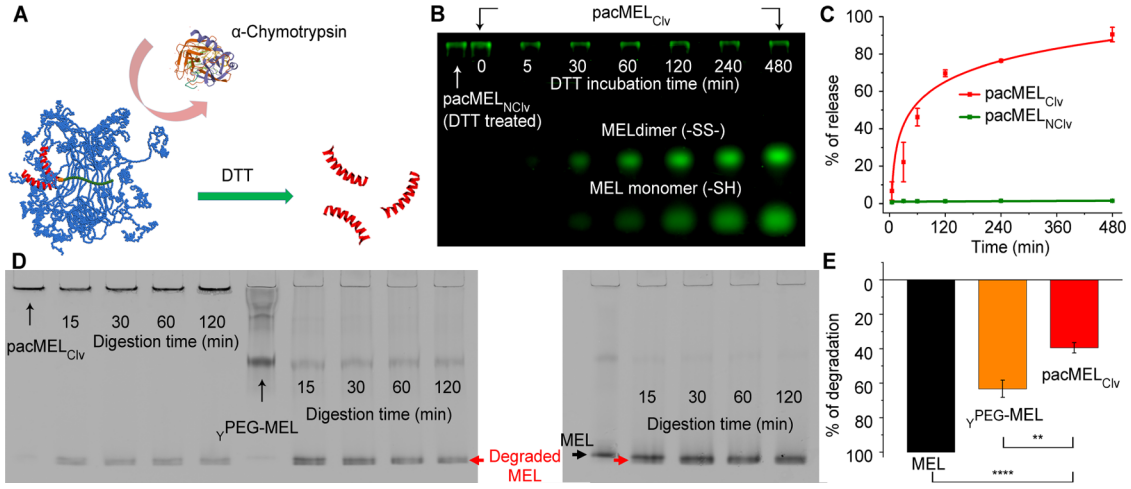

Figure 2. (A) Schematic illustration of the bioreductive release of MEL from pacMEL$_{Clv}$ and degradation of the MEL component by α-chymotrypsin (Protein Data Bank ID 2CHA). (B) Agarose gel electrophoresis (2%) of pacMEL$_{Clv}$ treated with 10 mM DTT with varying treatment times. (C) The release profile for pacMEL$_{Clv}$ was determined by gel band densitometry analysis. (D) PAGE showing α-chymotrypsin degradation of pacMEL$_{Clv}$, $_Y$PEG-MEL, and free MEL. The percentage of MEL degradation after 120 min of treatment is shown in (E). $^{**}P < 0.01$ and $^{****}P < 0.0001$ (two-tailed *t*-test).

activity, cytotoxicity, and liver damage. Collectively, we demonstrate a safer and pharmacologically superior form of the highly toxic peptide MEL, achieved using predominately PEG. The findings reported here make MEL a more appealing therapeutic agent for translational consideration and should expand the possibilities for the delivery of other types of narrow-therapeutic index drugs.

RESULTS AND DISCUSSION

Preparation and Characterization of pacMEL. To shield MEL from the biological environment, we designed a high-grafting-density bottlebrush PEG (degree of polymerization ∼30, M_w 271 kDa, Đ 1.27) with long side chains (M_n 10 kDa, Đ 1.05) as the carrier platform based on previous physiochemical and pharmacological findings.[23,25,26] pacMEL was synthesized via click reaction between the azide-functionalized bottlebrush polymer and dibenzocyclooctyne-functionalized MEL.[29−31] Unreacted PEG macromonomers and MEL were removed during the purification via aqueous gel permeation chromatography (GPC, Figures 1A and S4C). Because MEL works by forming a tetrameric complex and then binds to the phospholipid bilayer, it must be released from the polymer to regain activity.[25] Thus, a cysteine modification at the C-terminus of MEL was used to form a bioreductively cleavable disulfide linkage with the diblock bottlebrush copolymer (pacMEL$_{Clv}$). We also synthesized two negative controls: a non-cleavable conjugate, pacMEL$_{NClv}$, and a conjugate of a low PEG density (M_n = 40 kDa, Y-shaped PEG, each arm is 20 kDa, Đ 1.05), $_Y$PEG-MEL (Scheme 1).

The number of peptides per bottlebrush was determined to be 3.3 for pacMEL$_{NClv}$ and 2.6 for pacMEL$_{Clv}$ (Figure 1B; for details, see SI). The average MEL loading number for pacMEL$_{Clv}$ was verified by treatment with tris(2-carboxyethyl)-phosphine (TCEP) and subsequent GPC analysis (Figure S4B,C) to be 2.1 MEL per conjugate, which is approximately consistent with the dye-labeling method. Transmission electron microscopy (TEM) shows that pacMEL$_{Clv}$ exhibits a globular structure with a dry-state diameter of 23 ± 3 nm, which is in line with dynamic light scattering (DLS) analysis (a D_h of 34.1 ± 0.4 nm, Figure 1C,D). The observed globular morphology of pacMEL is the result of the collapse of the hydrophobic polynorbornene backbone in aqueous solution, which has been reported in other studies and simulations.[32,33] Considering the number of the side chains (DP_n ∼ 30) in our design, the polymer used in pacMEL has entered the bottlebrush regime and should offer stronger steric inhibition of external macromolecules than the slightly branched star polymers.[21,34] $_Y$PEG-MEL exhibits an expected smaller cumulant D_h of 21.0 ± 0.5 nm. ζ-potential measurements indicate that PEGylation reduces the overall positive charge of MEL, especially by the bottlebrush PEG; both the pacMELs exhibit a near-neutral ζ-potential (0.3 mV) compared with natural MEL (∼8 mV, Figure 1E).

Reductive Cleavage and Proteinase Stability. We first tested the bioreductive release of pacMEL$_{Clv}$, which offers a secondary tumor-targeting effect by releasing active MEL more readily at tumor sites in addition to the primary EPR effect. Glutathione levels are reported to be elevated in several human cancers, including NSCLC, which is used as a model to investigate the efficacy of pacMEL formulations (vide infra).[35,36] Dithiothreitol (DTT) [10 mM in phosphate-buffered saline (PBS)] was used to simulate the intracellular reducing environment in cancer cells, and agarose gel electrophoresis was used to monitor the release kinetics of MEL from the conjugate (Figure 2B). Using band densitometry analysis, a release profile is plotted as a function of incubation time. It is found that 50% MEL is released from pacMEL$_{Clv}$ during the first hour, and 80% release is achieved in ∼4 h (Figure 2C). The faster release kinetics relative to clearance (vide infra) suggests that the majority of conjugated MEL will become bioavailable as opposed to remaining in the prodrug form after clearance.

Next, we studied whether the bottlebrush PEG can shield MEL better than conventional PEG using a proteinase assay. In this assay, α-chymotrypsin, which can catalyze the hydrolysis of peptide bonds on the C-terminal side of tryptophan and leucine,[37] was used to treat the MEL-containing samples, and cleaved versus intact MEL can be quantified after polyacrylamide gel electrophoresis (PAGE, Figure 2D). Upon the addition of α-chymotrypsin, free MEL

https://doi.org/10.1021/acsami.1c14285
ACS Appl. Mater. Interfaces 2021, 13, 42533−42542

and $_{Y}$PEG-MEL were digested rapidly; the bands corresponding to intact MEL diminished significantly after 15 min. In contrast, the majority (~60%) of pacMEL$_{Clv}$ remain intact after 2 h (Figure 2E). These results suggest that the bottlebrush PEG can offer markedly better steric shielding than slightly branched PEG and in principle can more effectively inhibit unwanted interactions between MEL and various proteins/cells in the circulation system. Of note, α-chymotrypsin is a relatively small protein with a molecule weight of 25 kDa;[38] larger proteins are expected to be blocked against to an even greater extent by the bottlebrush polymer.

Cellular Uptake, Cytotoxicity, and Blood Compatibility. One may intuitively assume that the dense PEGylation associated with the bottlebrush polymer diminishes all forms of interactions with the cells including endocytosis. Nonetheless, our recent studies on bottlebrush PEGylated oligonucleotides suggest that the hydrophobic backbone of the bottlebrush polymer is responsible for a moderate amount of endocytosis, and in fact, the conjugates exhibit ~10-fold higher cell uptake compared to naked oligonucleotides.[39,40] It is therefore of curiosity to compare the cell uptake of free and PEGylated MEL forms. A human NSCLC cell line (NCI-H358) and an ovarian carcinoma cell line (SKOV3) are selected as models to study the cellular uptake activities. The uptake of free MEL in both cell lines is a fast and accelerating process (Figures 3A,B and S5A,B). It has been suggested that such unusual uptake is initiated first by electrostatic interactions of the cationic peptide with the negatively charged cell membrane, followed by plasma membrane poration, which enables subsequent fast and direct plasma membrane permeation.[12,41] For the PEGylated MELs, cell uptake rates are slower and more linear, which is consistent with an endocytosis mechanism.[42−44] Interestingly, the pacMELs are taken up more readily than $_{Y}$PEG-MEL, although the MEL component in the former is less exposed than in the latter. This phenomenon may be attributed to the hydrophobic effect of the polymer backbone, which promotes cell uptake.[45] The distinct cellular uptake characteristics of naked and PEGylated MELs are also corroborated by confocal microscopy. While free MEL exhibits very high cell-associated signals and a more diffused appearance of MEL's intracellular distribution (suggesting cytosol access, Figure 3C), PEGylated MELs show reduced uptake and a punctate pattern indicative of endosomal localization.[46]

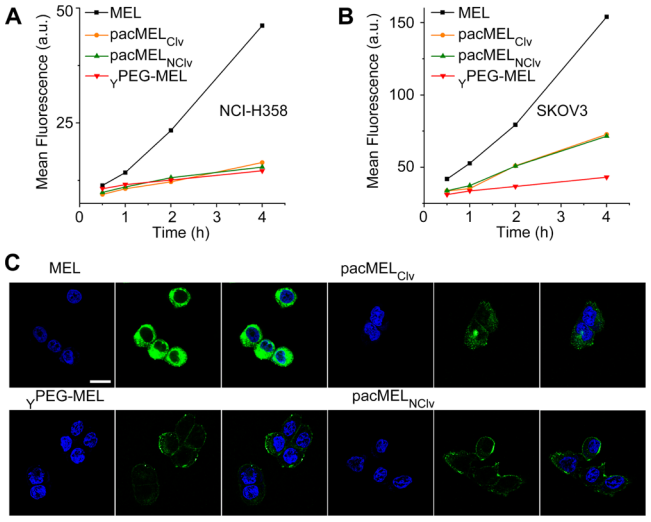

Figure 3. (A,B) Cellular uptake kinetics (as determined by flow cytometry) of cells treated with free MEL and PEGylated MELs (1 μM of MEL for 1−4 h). (C) Confocal microscopy images of NCI-H358 cells treated with samples containing 1 μM FITC-labeled MEL for 4 h. Cell nuclei are stained with DAPI (blue). The scale bar is 20 μm. Imaging settings were kept identical for all samples. However, signals for PEGylated samples were boosted 200% post imaging in order for details to be visible on-screen.

Because the cytotoxicity of MEL relies on the formation of its tetramer and the resulting lytic activity, the intracellular release of pacMEL$_{Clv}$ under bioreductive conditions can be evaluated by comparing its cytotoxicity with the non-cleavable pacMEL$_{NClv}$ and free MEL. We examined the cell viability using NCI-H358 and SKOV-3 cells after treatment with MEL-containing samples for 48 h. Remarkably, the cleavable conjugate, pacMEL$_{Clv}$, retained almost the entirety of the bioactivity of the free peptide (Figures 4A and S5C), suggesting efficient uptake and conversion from the prodrug to the active drug. It may be possible that the initial lytic activity of released MEL accelerated subsequent uptake of the conjugate over the course of 48 h. In contrast, the non-releasable pacMEL$_{NClv}$ exhibits no evident cytotoxicity. On the other hand, $_{Y}$PEG-MEL, which is non-cleavable, displays reduced but still apparent cytotoxicity, indicating that the normal PEGylation strategy cannot completely abolish the lytic activity of MEL.

Currently, the majority of peptide-based drugs are administrated through parenteral routes, including subcutaneous, intravenous, and intramuscular administration, as a result of their low oral bioavailability.[47,48] Therefore, to adopt MEL as a biopharmaceutical for passive solid tumor targeting, its behavior in the bloodstream is of great importance. It has been reported that MEL inhibits the activity of serine proteases, thus delaying blood coagulation.[11] We tested the anticoagulation properties of MEL and PEGylated MELs in human plasma using the activated partial thromboplastin time (aPTT) assay (Figure 4B). Free MEL shows pronounced interference with the coagulation cascade, doubling the coagulation times at a 20 μM MEL concentration. In contrast, pacMEL$_{Clv}$ displays a slight (statistically insignificant) increase in clotting times, while the bottlebrush PEG itself exhibits no measurable change. In comparison, both $_{Y}$PEG-MEL and a physical mixture of MEL/bottlebrush PEG result in similar anticoagulation effects to naked MEL, indicating that the architectural features of the bottlebrush are important in creating the steric hindrance necessary for inhibiting protein access.

Next, we examined MEL-induced hemolysis, a critical drawback of the peptide, by measuring the hemoglobin released from red blood cells (RBCs) (Figures 4C,D and S5D). Free MEL, expectedly, shows near-complete hemolysis of RBCs at 60 μM, with no visible precipitant after centrifugation. Even at 1 μM, 59% hemolysis was observed. All PEGylated samples exhibit greatly decreased hemolytic levels. $_{Y}$PEG-MEL (1 μM) displays reduced albeit non-negligible hemolysis (16%). Strikingly, both cleavable and non-cleavable pacMELs (1 μM) show almost no detectable hemolysis (<1%). The hemolytic activity of MEL for the cleavable conjugate can be partly restored by coincubating with 10 mM DTT (~65% lysis of RBCs, consistent with the expected level of MEL release) and fully restored when the coincubation time with DTT is increased to 8 h (DTT itself

https://doi.org/10.1021/acsami.1c14285
ACS Appl. Mater. Interfaces 2021, 13, 42533−42542

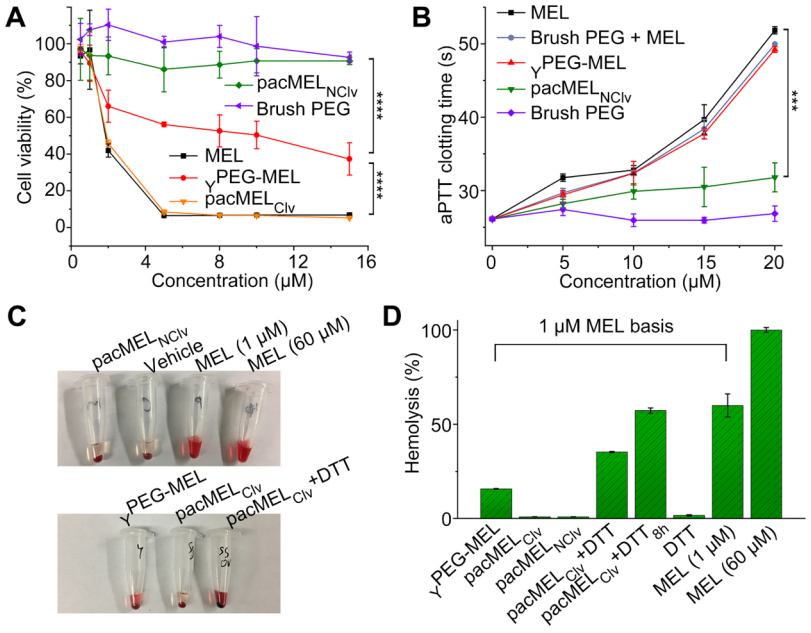

Figure 4. (A) Cell viability of NCI-H358 cells treated with MEL-containing samples and brush PEG for 48 h. (B) Activated partial thromboplastin times (aPTT) of human plasma treated with MEL-containing samples and controls. (C,D) Hemolysis assay of human RBCs treated with MEL-containing samples and controls. The percentage of hemolysis is determined by the spectrophotometric measurement of hemoglobin present in the supernatant of centrifuged red blood cell suspensions. ***$P < 0.001$ and ****$P < 0.0001$ (two-tailed t-test).

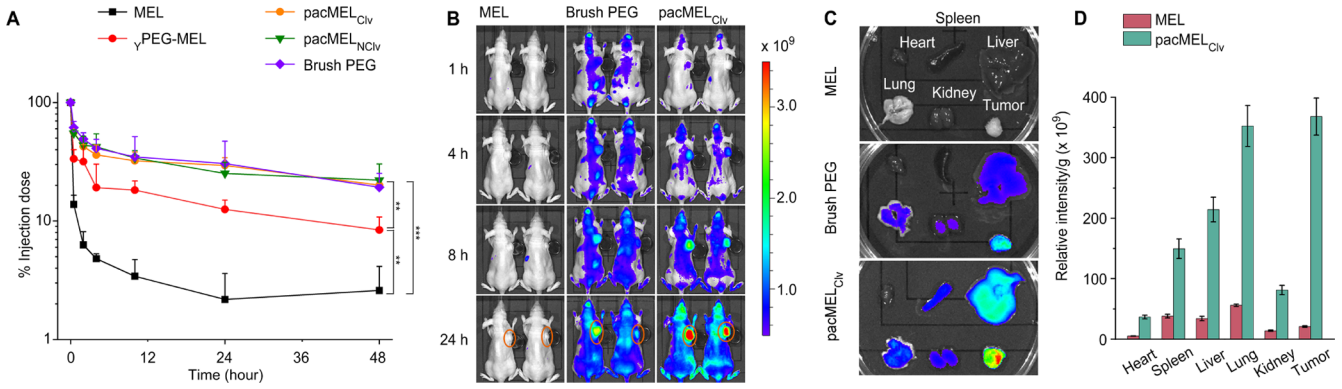

Figure 5. (A) Plasma pharmacokinetics of MEL-containing samples and the free bottlebrush polymer in C57BL/6 mice. (B) Near-IR imaging of BALB/c mice bearing NCI-H358 xenografts 24 h after i.v. injection with Cy5.5-labeled free MEL, pacMEL$_{Clv}$, and the bottlebrush polymer. Tumors are highlighted with orange circles. Of note, the fluorescence intensities for the bottlebrush polymer and pacMEL$_{Clv}$ are not directly comparable due to non-equal fluorescence at equal molar concentrations (1 Cy5.5 per brush polymer and ~2 Cy5.5 per pacMEL$_{Clv}$). (C,D) Ex vivo imaging of tumor and other major organs and the biodistribution profile determined from image analysis.

has no hemolytic property). The observation that pacMEL$_{Clv}$ shows essentially no hemolysis is consistent with the fact that mature RBCs do not endocytose and thus cannot release MEL intracellularly.[49] These results, together with enzymatic degradation, cytotoxicity, and blood coagulation studies (vide supra), paint an overall picture in which traditional PEGylation using linear or slightly branched PEG (e.g., $_{Y}$PEG) leaves the payload somewhat open to interactions with its intended or unintended target. The bottlebrush architecture, in contrast, imparts much stronger shielding to the payload against interactions with surrounding macromolecular or cellular species, making it more effective at suppressing unwanted side effects.

Pharmacokinetics, Biodistribution, and In Vivo Antitumor Efficacy. We anticipate that the biological stealth character of PEG and its dense arrangement in pacMEL will reduce the non-specific interactions between MEL and serum proteins and thereby minimize clearance by the mononuclear phagocyte system (MPS).[50] In addition, the large overall size of pacMEL (~300 kDa) should bypass rapid renal clearance.[51,52] These properties should in turn enhance plasma pharmacokinetics, which has been shown to favorably correlate with the nanomedicine's ability to passively accumulate in the mice tumor tissues through extravasation from the microvasculature (EPR effect).[53−55] To evaluate the plasma pharmacokinetics of the pacMELs, we administered pacMELs, free MEL, and the bottlebrush polymer at equal peptide/polymer concentrations to immunocompetent C57BL/6 mice via the tail vein. The MEL component is labeled with a Cy5.5 dye; in the case of the free brush polymer, the dye is directly attached to the polymer (~1.0 Cy5.5 per bottlebrush polymer). Blood samples at a series of predetermined time points up to 48 h were collected and analyzed (Figure 5A). Fitting the pharmacokinetic data using a two-compartment

https://doi.org/10.1021/acsami.1c14285
ACS Appl. Mater. Interfaces 2021, 13, 42533−42542

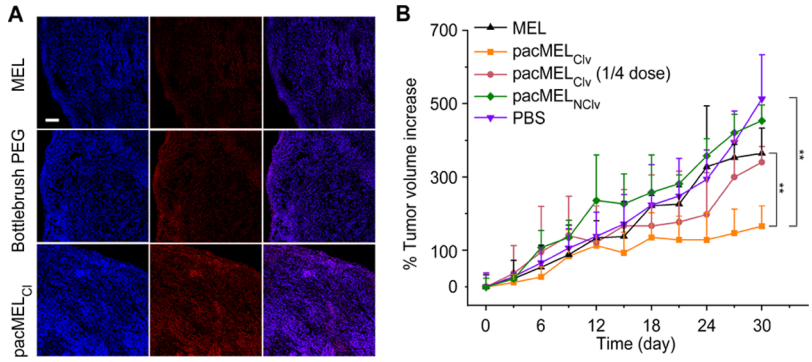

Figure 6. (A) Confocal microscopy images of NCI-H358 tumor cryosections following i.v. injection, showing deep tumor penetration. Blue: cell nuclei stained with DAPI. The scale bar is 100 μm. (B) Tumor volume change in the course of a 30 day treatment.

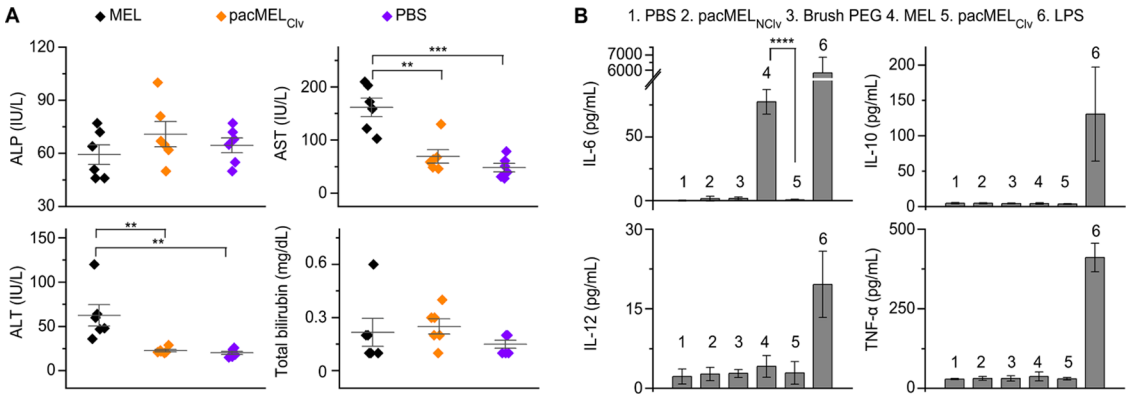

Figure 7. (A) Hepatic damage indicators (ALP, ASP, ALT, and total bilirubin) in the serum and (B) cytokine levels (IL-6, IL-10, IL-12, and TNF-α) in immunocompetent mice (C57BL/6) after three doses of pacMEL$_{Clv}$ and controls (3 mg/kg MEL basis). $^{**}P < 0.01$, $^{***}P < 0.001$, $^{****}P < 0.0001$ (two-tailed t-test).

model, it is apparent that all bottlebrush polymer-containing samples exhibit a similar profile, in which the particles quickly distribute into tissues with distribution half-lives ($t_{1/2\alpha}$) around 15 min and are cleared very slowly with elimination half-lives ($t_{1/2\beta}$) around 15 h. There was still ~20% of the injected dose remaining in blood circulation after 48 h of injection. In contrast, naked MEL was rapidly cleared, likely via the kidney, with $t_{1/2\alpha}$ and $t_{1/2\beta}$ of 0.48 and 43 min, respectively, which suggests low drug utilization. As a result, pacMELs experience substantially improved blood availability compared to free MEL [~10-fold higher the area under the curve ($AUC_{pacMEL,\infty}/AUC_{MEL,\infty}$ = 10)]. While $_{Y}$PEG-MEL exhibited longer blood circulation times than the free MEL, the improvement is not evident when compared with the pacMELs or the bottlebrush polymer. Given the inferior in vitro and pharmacokinetics performance, $_{Y}$PEG-MEL is not included in subsequent in vivo tests. All pharmacokinetic parameters are summarized in Table S1.

Fluorescence imaging of both live animals and dissected major organs/tumors 24 h post injection shows generally much stronger signals in mice injected with bottlebrush polymer-containing samples than those receiving free MEL (Figure 5B,C). Importantly, pacMELs resulted in significantly improved tumor uptake (18.4-fold higher compared to free MEL), likely via the EPR effect (Figure 5D). Notably, the free MEL-treated group shows low tumor versus spleen (0.55) and tumor versus liver (0.61) ratios, as determined by the relative fluorescence intensities, suggesting potential systemic toxicity, while these values for pacMEL$_{Clv}$ are 2.46 (spleen) and 1.42 (liver). Similar results are observed for the bottlebrush polymer (Figure S6). We further examined the tumor penetration depth by confocal microscopy of cryosectioned tumor slices that are stained with 4′,6-diamidino-2-phenylindole (DAPI, Figure 6A). It is found that significant MEL signals are present throughout the sliced tumor section of pacMEL$_{Clv}$-treated mice, similar to that of bottlebrush PEG-treated mice. These data clearly show that the bottlebrush polymer can effectively alleviate the fast clearance of naked MEL, achieve prolonged systematic circulation, and impart the tumor accumulation and penetration properties to the embedded MEL.

To evaluate the antitumor efficacy of pacMEL, we established xenografts of NCI-H358 cells in athymic nude mice. Mice received tail-vein injections of PBS, free MEL, pacMEL$_{Clv}$ (normal and 1/4 dose), and pacMEL$_{NClv}$ every 3 days at a dosage of 3 mg/kg (MEL-basis). Dosage is determined based on the reported median lethal dose (LD_{50}) of intravenously (i.v.) delivered naked MEL for mice, which is 4 mg/kg.[56] By day 30, tumors in vehicle-treated mice have grown to 453% of their original sizes. Despite a near-LD_{50} dosage, free MEL did not lead to statistically meaningful repression of tumor growth relative to the negative control, likely because tumor-associated MEL levels have yet to reach cytotoxic concentrations. In contrast, pacMEL$_{Clv}$ at the identical MEL dosage resulted in a significant decrease in tumor growth (165%, Figure 6B), which is attributed to improved pharmacokinetics and tumor localization. At 1/4 dosage, however, the conjugate was not as effective. Although pacMEL$_{Clv}$ does not lead to tumor stasis or regression at the

https://doi.org/10.1021/acsami.1c14285
ACS Appl. Mater. Interfaces 2021, 13, 42533−42542

tested concentrations, there is a clear dosage response, and the conjugate may have a higher mean tolerable dosage to allow for more effective treatment, given its modified biodistribution profile and much reduced hemolytic activity. Indeed, while naked MEL caused alarming increases in alanine trans-aminase (ALT) and aspartate aminotransferase in C57BL/6 mice, indicative of liver damage, pacMEL$_{Clv}$-treated mice exhibited no such increases and no noticeable changes in additional important biochemical and hematological parameters (Figures 7A and S7). Staining sectioned major organs with hematoxylin and eosin (H&E) revealed no abnormal histological changes for mice treated with all samples (Figure S8). It has been shown that despite causing elevated liver enzymes and sometimes deaths, naked MEL may not produce observable histological evidence of toxicity.[57] Further, free MEL induces activation of interleukin-6 (IL-6), as determined in a cytokine analysis using the enzyme-linked immunosorbent assay (ELISA, Figure 7B). The pacMELs and the bottlebrush polymer, on the other hand, do not induce evident differences in the levels of IL-6, IL-10, IL-12, and tumor necrosis factor α (TNF-α). Collectively, these results show that the bottlebrush polymer is able to impart a more desirable pharmacological and safety profile to MEL while enhancing bioavailability and specific toxicity to the tumor.

CONCLUSIONS

MEL and other narrow therapeutic index agents with strong non-specific interactions face a difficult compromise: the combined challenges of poor accumulation in target tissues and rapid clearance by the liver and/or the kidney require larger doses of the agent, but increasing doses would lead to elevated toxicity and/or immunological responses. These challenges limit the therapeutic window between a therapy that is efficacious and one that is toxic, increase the costs to patients, and very often limit the places in the body where effective therapies can be developed. The results reported herein provide tantalizing evidence that the bottlebrush polymer may be able to solve this conundrum. The high-density arrangement of the PEG side chains of the bottlebrush polymer provides extraordinary steric shielding to the embedded MEL compared to "normal" PEG, allowing the conjugate to bypass non-specific interactions with various proteins and cells while in circulation, thereby reducing coagulopathy, hemolysis, and capture by the MPS. The large size of pacMEL enables effective evasion from renal clearance, which significantly prolongs blood circulation times and gives rise to better utilization of the active drug, a more favorable biodistribution profile, and enhanced passive targeting of tumor tissues. Importantly, these pharmacological improvements are realized using a well-defined, single-entity molecular agent that consists predominantly of PEG, which is a safe material having been adopted in a large number of biopharmaceuticals. The simplicity makes these structures more amenable to large-scale manufacturing, quality control, and room-temperature storage compared with self-assembled, dynamic carrier systems that rely on non-covalent supramolecular interactions (such as extracellular vesicles, micelles, and so forth), which should elevate the translational potential of the conjugate.

In summary, we report a novel form of PEGylated MEL that utilizes the high grafting density of the bottlebrush polymer to achieve improved steric shielding. The conjugate exhibits vastly superior biopharmaceutical properties compared to naked MEL as well as PEGylated MEL containing a conventional, slightly branched PEG. This approach makes MEL a much more attractive anticancer drug candidate by abolishing its excessive hemolytic activity, prolonging plasma pharmacokinetics, and improving tumor uptake. Of significance, the bottlebrush system should be broadly applicable to a variety of therapeutic candidates whose biopharmaceutical properties and therapeutic indices are considered unsatisfactory.

MATERIALS AND METHODS

Animal protocols were approved by the Institutional Animal Care and Use Committee of Northeastern University and carried out in accordance with the approved guidelines.

Biodistribution. Fluorescence whole-animal and ex vivo tissue imaging were used to assess the biodistribution of test agents in mice. NCI-H358 cells were used to establish subcutaneous xenografts. Cells (2.0×10^6) suspended in PBS solution (200 μL) were inoculated in female athymic nude mice subcutaneously. When the tumor size reaches ~200 mm^3, mice were randomly divided into three groups (n = 2) and administrated with an equivalent dose of MEL (3 mg/kg) or the bottlebrush polymer (equal molar concentration as pacMEL$_{Clv}$) via tail-vein injection in 200 μL of PBS solution. Fluorescence imaging was performed using an animal imaging system (IVIS Lumina II imaging system, Caliper Life Sciences Inc., MA, USA) at 1, 4, 8, and 24 h after injection. Mice were euthanized 24 h after injection, and major organs were collected for imaging and biodistribution analysis. Tumor tissues were frozen in an optimal cutting temperature compound (Fisher Scientific Inc., USA) and cut into 8 μm thick sections using a cryostat for agents' tumor penetration depth study. DAPI was used to stain the nuclei, and the tumor sections were imaged using confocal microscopy (Carl Zeiss Ltd., Cambridge, UK).

Pharmacokinetics. Immunocompetent mice (C57BL/6) were randomly divided into four groups (n = 5): free MEL, pacMELs, and the bottlebrush polymer [MEL is labeled with Cy5.5; equal MEL basis (6 nmol); identical polymer molar amount as pacMEL$_{Clv}$]. Samples were injected intravenously via the tail vein, and blood samples were collected from the submandibular region at varying time points (30 min, 2, 4, 10, 24, and 48 h) using vacutainer blood collection tubes containing sodium heparin (Becton, Dickinson and Company, US). Plasma at different time points was obtained by centrifugation at 3000 rpm 4 °C for 15 min. The clear plasma samples were then transferred into a 96-well optical bottom plate (Fisher Scientific Inc., US) for fluorescence readout (ex = 620 nm, em = 680 nm) using a Synergy Neo2 microplate reader (BioTek Instruments Inc., US). The average values of each time point were then plotted against the standard curve prepared by sequential dilution with freshly collected mouse plasma.

Tumor Growth Inhibition. The mouse xenograft model (NCI-H358 cell line) was established in athymic nude mice (vide supra). When the tumor size reached ~100 mm^3, tumor-bearing mice were randomly divided into five groups (n = 4): free MEL (3 mg/kg), pacMEL$_{Clv}$ (dose 3 mg/kg), low-dose pacMEL$_{Clv}$ (0.75 mg/kg), brush polymer (identical polymer molar amount as normal dose pacMELs), and PBS control. Samples and controls were injected via the tail vein every 3rd day for 30 days. The weight of mice (Figure S9) and the volume of tumors were recorded before each injection and at the end of 10 treatments. Tumor growth inhibition was evaluated by measuring the tumor volume at different time points ($V = 0.5 \times a \times b^2$; a: long diameter, b: short diameter).

Innate Immune Response. Innate immune response was evaluated in female C57BL/6 mice. The mice were randomly divided into six groups (n = 5): free MEL (3 mg/kg), pacMELs (equal MEL basis), bottlebrush polymer (identical polymer amount as pacMELs), and negative (vehicle, PBS) and positive (lipopolysaccharide, 15 μg per mouse) controls. Blood samples were collected for cytokine analysis 4 h after injection. TNF-α, IL-6, IL-10, and IL-12 were analyzed using the corresponding ELISA kits (R&D Systems Inc., MN, USA).

Hemanalysis and Biochemical Analyses. Blood analyses were assessed in female C57BL/6 mice. Mice were randomly divided into

https://doi.org/10.1021/acsami.1c14285
ACS Appl. Mater. Interfaces 2021, 13, 42533−42542

three groups (n = 6): free MEL (3 mg/kg), pacMEL$_{Clv}$ (equal MEL basis), and PBS control. Samples and the control were injected via the tail vein once every 3 days for a total of three doses. Blood samples were collected 2 days after the last injection (day 11) from the submandibular region. Ethylenediaminetetraacetic acid-treated whole blood samples were used to perform the complete blood count panel test, and serum samples were collected for hepatic damage evaluation.

Statistics. All experiments were repeated at least three times unless otherwise indicated. Data are presented as means ± SD. Statistical significance was evaluated by using a two-tailed t-test when only two groups were compared. Statistical significance was set at $^{**}P < 0.01$, $^{***}P < 0.001$, or $^{****}P < 0.0001$.

■ ASSOCIATED CONTENT

Supporting Information

The Supporting Information is available free of charge at https://pubs.acs.org/doi/10.1021/acsami.1c14285.

Synthesis and characterization of PEGylated MELs; enzymatic degradation of MEL-containing samples; in vitro experiments; in vivo antitumor activity; and initial biocompatibility evaluation of MEL-containing samples (PDF)

■ AUTHOR INFORMATION

Corresponding Authors

Xueguang Lu − *David H. Koch Institute for Integrative Cancer Research, Massachusetts Institute of Technology, Cambridge, Massachusetts 02139, United States;* Present Address: Key Laboratory of Colloid, Interface and Chemical Thermodynamics, Institute of Chemistry, Chinese Academy of Sciences, Beijing 100190, P. R. China; Email: xueguang@mit.edu

Ke Zhang − *Departments of Chemistry and Chemical Biology, Chemical Engineering, and Bioengineering, Northeastern University, Boston, Massachusetts 02115, United States;* orcid.org/0000-0002-8142-6702; Email: k.zhang@northeastern.edu

Authors

Fei Jia − *Departments of Chemistry and Chemical Biology, Chemical Engineering, and Bioengineering, Northeastern University, Boston, Massachusetts 02115, United States*

Peiru Chen − *Departments of Chemistry and Chemical Biology, Chemical Engineering, and Bioengineering, Northeastern University, Boston, Massachusetts 02115, United States*

Dali Wang − *Departments of Chemistry and Chemical Biology, Chemical Engineering, and Bioengineering, Northeastern University, Boston, Massachusetts 02115, United States*

Yehui Sun − *Departments of Chemistry and Chemical Biology, Chemical Engineering, and Bioengineering, Northeastern University, Boston, Massachusetts 02115, United States*

Mengqi Ren − *Departments of Chemistry and Chemical Biology, Chemical Engineering, and Bioengineering, Northeastern University, Boston, Massachusetts 02115, United States*

Yuyan Wang − *Departments of Chemistry and Chemical Biology, Chemical Engineering, and Bioengineering, Northeastern University, Boston, Massachusetts 02115, United States*

Xueyan Cao − *Departments of Chemistry and Chemical Biology, Chemical Engineering, and Bioengineering, Northeastern University, Boston, Massachusetts 02115, United States;* orcid.org/0000-0003-4366-8943

Lei Zhang − *Departments of Chemistry and Chemical Biology, Chemical Engineering, and Bioengineering, Northeastern University, Boston, Massachusetts 02115, United States*

Yang Fang − *Departments of Chemistry and Chemical Biology, Chemical Engineering, and Bioengineering, Northeastern University, Boston, Massachusetts 02115, United States*

Xuyu Tan − *Departments of Chemistry and Chemical Biology, Chemical Engineering, and Bioengineering, Northeastern University, Boston, Massachusetts 02115, United States*

Hao Lu − *Departments of Chemistry and Chemical Biology, Chemical Engineering, and Bioengineering, Northeastern University, Boston, Massachusetts 02115, United States*

Jiansong Cai − *Departments of Chemistry and Chemical Biology, Chemical Engineering, and Bioengineering, Northeastern University, Boston, Massachusetts 02115, United States*

Complete contact information is available at: https://pubs.acs.org/10.1021/acsami.1c14285

Author Contributions

§F.J. and P.C. contributed equally. All authors have given approval to the final version of the manuscript.

Funding

Research reported in this publication was supported by the National Institute of General Medical Sciences (1R01GM121612), the National Cancer Institute (1R01CA251730), and the National Science Foundation (DMR award no. 2004947).

Notes

The authors declare no competing financial interest.

■ ACKNOWLEDGMENTS

We thank the Institute for Chemical Imaging of Living System at Northeastern University for consultation and imaging support.

■ REFERENCES

(1) Henninot, A.; Collins, J. C.; Nuss, J. M. The Current State of Peptide Drug Discovery: Back to the Future? *J. Med. Chem.* **2018**, *61*, 1382−1414.

(2) Muttenthaler, M.; King, G. F.; Adams, D. J.; Alewood, P. F. Trends in Peptide Drug Discovery. *Nat. Rev. Drug Discovery* **2021**, *20*, 309.

(3) Fosgerau, K.; Hoffmann, T. Peptide Therapeutics: Current Status and Future Directions. *Drug Discov. Today* **2015**, *20*, 122−128.

(4) Choi, J. H.; Jang, A. Y.; Lin, S.; Lim, S.; Kim, D.; Park, K.; Han, S.-M.; Yeo, J.-H.; Seo, H. S. Melittin, a Honeybee Venom-derived Antimicrobial Peptide, May Target Methicillin-resistant Staphylococcus Aureus. *Mol. Med. Rep.* **2015**, *12*, 6483−6490.

(5) Gajski, G.; Garaj-Vrhovac, V. Melittin: A lytic peptide with anticancer properties. *Toxicol. Pharmacol.* **2013**, *36*, 697−705.

(6) Schweizer, F. Cationic Amphiphilic Peptides with Cancer-Selective Toxicity. *Eur. J. Pharmacol.* **2009**, *625*, 190−194.

(7) Fadnes, B.; Rekdal, Ø.; Uhlin-Hansen, L. The Anticancer Activity of Lytic Peptides Is Inhibited by Heparan Sulfate on the Surface of the Tumor Cells. *BMC Canc.* **2009**, *9*, 183.

(8) Soman, N. R.; Lanza, G. M.; Heuser, J. M.; Schlesinger, P. H.; Wickline, S. A. Synthesis and Characterization of Stable Fluorocarbon Nanostructures as Drug Delivery Vehicles for Cytolytic Peptides. *Nano Lett.* **2008**, *8*, 1131−1136.

(9) Memariani, H.; Memariani, M.; Moravvej, H.; Shahidi-Dadras, M. Melittin: A Venom-Derived Peptide with Promising Anti-Viral Properties. *Eur. J. Clin. Microbiol. Infect. Dis.* **2020**, *39*, 5−17.

(10) Bacalum, M.; Radu, M. Cationic Antimicrobial Peptides Cytotoxicity on Mammalian Cells: An Analysis Using Therapeutic Index Integrative Concept. *Int. J. Pept. Res. Ther.* **2015**, *21*, 47−55.
(11) Lee, J.; Park, J.; Yeom, J.; Han, E. H.; Lim, Y.-H. Inhibitory Effect of Bee Venom on Blood Coagulation via Anti-Serine Protease Activity. *J. Asia Pac. Entomol.* **2017**, *20*, 599−604.
(12) Lee, M.-T.; Sun, T.-L.; Hung, W.-C.; Huang, H. W. Process of Inducing Pores in Membranes by Melittin. *Proc. Natl. Acad. Sci.* **2013**, *110*, 14243−14248.
(13) Nishikawa, H.; Kitani, S. Gangliosides Inhibit Bee Venom Melittin Cytotoxicity but Not Phospholipase A2-Induced Degranulation in Mast Cells. *Toxicol. Appl. Pharmacol.* **2011**, *252*, 228−236.
(14) Vellard, M. The Enzyme as Drug: Application of Enzymes as Pharmaceuticals. *Curr. Opin. Biotechnol.* **2003**, *14*, 444−450.
(15) Harris, J. M.; Chess, R. B. Effect of Pegylation on Pharmaceuticals. *Nat. Rev. Drug Discov.* **2003**, *2*, 214−221.
(16) Pasut, G.; Veronese, F. M. State of the Art in PEGylation: The Great Versatility Achieved after Forty Years of Research. *J. Controlled Release* **2012**, *161*, 461−472.
(17) Peng, H. T.; Huang Huang, H.; Shek, P. N.; Charbonneau, S.; Blostein, M. D. PEGylation of Melittin: Structural Characterization and Hemostatic Effects. *J. Bioact. Compat Polym.* **2010**, *25*, 75−97.
(18) Leitgeb, A.; Wappel, J.; Slugovc, C. The ROMP Toolbox Upgraded. *Polymer* **2010**, *51*, 2927−2946.
(19) Xie, M.; Dang, J.; Han, H.; Wang, W.; Liu, J.; He, X.; Zhang, Y. Well-Defined Brush Copolymers with High Grafting Density of Amphiphilic Side Chains by Combination of ROP, ROMP, and ATRP. *Macromolecules* **2008**, *41*, 9004−9010.
(20) Medina, J. M.; Ko, J. H.; Maynard, H. D.; Garg, N. K. Expanding the ROMP Toolbox: Synthesis of Air-Stable Benzonorbornadiene Polymers by Aryne Chemistry. *Macromolecules* **2017**, *50*, 580−586.
(21) Xia, Y.; Li, Y.; Burts, A. O.; Ottaviani, M. F.; Tirrell, D. A.; Johnson, J. A.; Turro, N. J.; Grubbs, R. H. EPR Study of Spin Labeled Brush Polymers in Organic Solvents. *J. Am. Chem. Soc.* **2011**, *133*, 19953−19959.
(22) Vohidov, F.; Andersen, J. N.; Economides, K. D.; Shipitsin, M. V.; Burenkova, O.; Ackley, J. C.; Vangamudi, B.; Nguyen, H. V.-T.; Gallagher, N. M.; Shieh, P.; Golder, M. R.; Liu, J.; Dahlberg, W. K.; Ehrlich, D. J. C.; Kim, J.; Kristufek, S. L.; Huh, S. J.; Neenan, A. M.; Baddour, J.; Paramasivan, S.; de Stanchina, E.; KC, G.; Turnquist, D. J.; Saucier-Sawyer, J. K.; Kopesky, P. W.; Brady, S. W.; Jessel, M. J.; Reiter, L. A.; Chickering, D. E.; Johnson, J. A.; Blume-Jensen, P. Design of BET Inhibitor Bottlebrush Prodrugs with Superior Efficacy and Devoid of Systemic Toxicities. *J. Am. Chem. Soc.* **2021**, *143*, 4714−4724.
(23) Jia, F.; Lu, X.; Tan, X.; Wang, D.; Cao, X.; Zhang, K. Effect of PEG Architecture on the Hybridization Thermodynamics and Protein Accessibility of PEGylated Oligonucleotides. *Angew. Chem., Int. Ed.* **2017**, *56*, 1239−1243.
(24) Jia, F.; Lu, X.; Wang, D.; Cao, X.; Tan, X.; Lu, H.; Zhang, K. Depth-Profiling the Nuclease Stability and the Gene Silencing Efficacy of Brush-Architectured Poly(Ethylene Glycol)−DNA Conjugates. *J. Am. Chem. Soc.* **2017**, *139*, 10605−10608.
(25) Wang, D.; Lin, J.; Jia, F.; Tan, X.; Wang, Y.; Sun, X.; Cao, X.; Che, F.; Lu, H.; Gao, X.; Shimkonis, J. C.; Nyoni, Z.; Lu, X.; Zhang, K. Bottlebrush-Architectured Poly(Ethylene Glycol) as an Efficient Vector for RNA Interference in Vivo. *Sci. Adv.* **2019**, *5*, No. eaav9322.
(26) Lu, X.; Tran, T.-H.; Jia, F.; Tan, X.; Davis, S.; Krishnan, S.; Amiji, M. M.; Zhang, K. Providing Oligonucleotides with Steric Selectivity by Brush-Polymer-Assisted Compaction. *J. Am. Chem. Soc.* **2015**, *137*, 12466−12469.
(27) Shieh, P.; Nguyen, H. V.-T.; Johnson, J. A. Tailored Silyl Ether Monomers Enable Backbone-Degradable Polynorbornene-Based Linear, Bottlebrush and Star Copolymers Through ROMP. *Nat. Chem.* **2019**, *11*, 1124−1132.
(28) Shieh, P.; Zhang, W.; Husted, K. E. L.; Kristufek, S. L.; Xiong, B.; Lundberg, D. J.; Lem, J.; Veysset, D.; Sun, Y.; Nelson, K. A.; Plata, D. L.; Johnson, J. A. Cleavable Comonomers Enable Degradable, Recyclable Thermoset Plastics. *Nature* **2020**, *583*, 542−547.
(29) Johnson, J. A.; Lu, Y. Y.; Burts, A. O.; Xia, Y.; Durrell, A. C.; Tirrell, D. A.; Grubbs, R. H. Drug-Loaded, Bivalent-Bottle-Brush Polymers by Graft-through ROMP. *Macromolecules* **2010**, *43*, 10326−10335.
(30) Bates, C. M.; Chang, A. B.; Momčilović, N.; Jones, S. C.; Grubbs, R. H. ABA Triblock Brush Polymers: Synthesis, Self-Assembly, Conductivity, and Rheological Properties. *Macromolecules* **2015**, *48*, 4967−4973.
(31) Xu, L.; Kuan, S. L.; Weil, T. Contemporary Approaches for Site-Selective Dual Functionalization of Proteins. *Angew. Chem., Int. Ed.* **2021**, *60*, 13757−13777.
(32) Zhang, M.; Müller, A. H. E. Cylindrical Polymer Brushes. *J. Polym. Sci., Part A: Polym. Chem.* **2005**, *43*, 3461−3481.
(33) Jia, F.; Kubiak, J. M.; Onoda, M.; Wang, Y.; Macfarlane, R. J. Design and Synthesis of Quick Setting Non-Swelling Hydrogels via Brush Polymers. *Adv. Sci.* **2021**, *8*, 2100968.
(34) Pesek, S. L.; Li, X.; Hammouda, B.; Hong, K.; Verduzco, R. Small-Angle Neutron Scattering Analysis of Bottlebrush Polymers Prepared via Grafting-Through Polymerization. *Macromolecules* **2013**, *46*, 6998−7005.
(35) Blair, S. L.; Heerdt, P.; Sachar, S.; Abolhoda, A.; Hochwald, S.; Cheng, H.; Burt, M. Glutathione Metabolism in Patients with Non-Small Cell Lung Cancers. *Cancer Res.* **1997**, *57*, 152−155.
(36) Gamcsik, M. P.; Kasibhatla, M. S.; Teeter, S. D.; Colvin, O. M. Glutathione Levels in Human Tumors. *Biomarkers* **2012**, *17*, 671−691.
(37) Ingles, D.; Knowles, J. Specificity and Stereospecificity of α-Chymotrypsin. *Biochem. J.* **1967**, *104*, 369−377.
(38) Kumar, A.; Venkatesu, P. Overview of the Stability of α-Chymotrypsin in Different Solvent Media. *Chem. Rev.* **2012**, *112*, 4283−4307.
(39) Lu, X.; Jia, F.; Tan, X.; Wang, D.; Cao, X.; Zheng, J.; Zhang, K. Effective Antisense Gene Regulation via Noncationic, Polyethylene Glycol Brushes. *J. Am. Chem. Soc.* **2016**, *138*, 9097−9100.
(40) Wang, D.; Lu, X.; Jia, F.; Tan, X.; Sun, X.; Cao, X.; Wai, F.; Zhang, C.; Zhang, K. Precision Tuning of DNA- and Poly(Ethylene Glycol)-Based Nanoparticles via Coassembly for Effective Antisense Gene Regulation. *Chem. Mater.* **2017**, *29*, 9882−9886.
(41) Yang, L.; Harroun, T. A.; Weiss, T. M.; Ding, L.; Huang, H. W. Barrel-Stave Model or Toroidal Model? A Case Study on Melittin Pore. *Biophys. J.* **2001**, *81*, 1475−1485.
(42) Cao, X.; Lu, X.; Wang, D.; Jia, F.; Tan, X.; Corley, M.; Chen, X.; Zhang, K. Modulating the Cellular Immune Response of Oligonucleotides by Brush Polymer-Assisted Compaction. *Small* **2017**, *13*, 1701432.
(43) Choi, C. H. J.; Hao, L.; Narayan, S. P.; Auyeung, E.; Mirkin, C. A. Mechanism for the Endocytosis of Spherical Nucleic Acid Nanoparticle Conjugates. *Proc. Natl. Acad. Sci.* **2013**, *110*, 7625−7630.
(44) McMahon, H. T.; Boucrot, E. Molecular Mechanism and Physiological Functions of Clathrin-Mediated Endocytosis. *Nat. Rev. Mol. Cell Biol.* **2011**, *12*, 517−533.
(45) Yu, C.; He, B.; Xiong, M.-H.; Zhang, H.; Yuan, L.; Ma, L.; Dai, W.-B.; Wang, J.; Wang, X.-L.; Wang, X.-Q.; Zhang, Q. The Effect of Hydrophilic and Hydrophobic Structure of Amphiphilic Polymeric Micelles on Their Transport in Epithelial MDCK Cells. *Biomaterials* **2013**, *34*, 6284−6298.
(46) Urbé, S.; Mills, I. G.; Stenmark, H.; Kitamura, N.; Clague, M. J. Endosomal Localization and Receptor Dynamics Determine Tyrosine Phosphorylation of Hepatocyte Growth Factor-Regulated Tyrosine Kinase Substrate. *Mol. Cell. Biol.* **2000**, *20*, 7685−7692.
(47) Bruno, B. J.; Miller, G. D.; Lim, C. S. Basics and Recent Advances in Peptide and Protein Drug Delivery. *Ther. Deliv.* **2013**, *4*, 1443−1467.
(48) Patel, A.; Patel, M.; Yang, X.; Mitra, A. Recent Advances in Protein and Peptide Drug Delivery: A Special Emphasis on Polymeric Nanoparticles. *Protein Pept. Lett.* **2014**, *21*, 1102−1120.

https://doi.org/10.1021/acsami.1c14285
ACS Appl. Mater. Interfaces 2021, 13, 42533−42542

(49) Wadhwa, R.; Aggarwal, T.; Thapliyal, N.; Kumar, A.; Yadav, P.; Kumari, V.; Reddy, B. S. C.; Chandra, P.; Maurya, P. K. Red Blood Cells as an Efficient in Vitro Model for Evaluating the Efficacy of Metallic Nanoparticles. *3 Biotech* **2019**, *9*, 279.
(50) Halma, C.; Daha, M. R.; van Es, L. a. V. In Vivo Clearance by the Mononuclear Phagocyte System in Humans: An Overview of Methods and Their Interpretation. *Clin. Exp. Immunol.* **1992**, *89*, 1−7.
(51) Ruggiero, A.; Villa, C. H.; Bander, E.; Rey, D. A.; Bergkvist, M.; Batt, C. A.; Manova-Todorova, K.; Deen, W. M.; Scheinberg, D. A.; McDevitt, M. R. Paradoxical Glomerular Filtration of Carbon Nanotubes. *Proc. Natl. Acad. Sci.* **2010**, *107*, 12369−12374.
(52) Meibohm, B.; Zhou, H. Characterizing the Impact of Renal Impairment on the Clinical Pharmacology of Biologics. *J. Clin. Pharmacol.* **2012**, *52*, 54S−62S.
(53) Fang, J.; Nakamura, H.; Maeda, H. The EPR Effect: Unique Features of Tumor Blood Vessels for Drug Delivery, Factors Involved, and Limitations and Augmentation of the Effect. *Adv. Drug Deliv. Rev.* **2011**, *63*, 136−151.
(54) Greish, K. Enhanced Permeability and Retention (EPR) Effect for Anticancer Nanomedicine Drug Targeting. *Methods Mol. Biol.* **2010**, *624*, 25−37.
(55) Danhier, F. To Exploit the Tumor Microenvironment: Since the EPR Effect Fails in the Clinic, What Is the Future of Nanomedicine? *J. Controlled Release* **2016**, *244*, 108−121.
(56) Habermann, E.; Zeuner, G. Comparative Studies of Native and Synthetic Melittins. *Naunyn-Schmiedeberg's Arch. Pharmacol.* **1971**, *270*, 1−9.
(57) Saeed, W. S. E.; Khalil, E. a. G. Toxic Effects and Safety of Bee Venom Protein [Melittin] in Mice: Search for Natural Vaccine Adjuvants. *J. Nat. Prod. Resour.* **2017**, *3*, 111−114.

https://doi.org/10.1021/acsami.1c14285
ACS Appl. Mater. Interfaces 2021, 13, 42533−42542